The effects of strain and composition on the conduction-band offset of direct band gap type-I GeSn/GeSnSi quantum dots for CMOS compatible mid-IR light source

Qimiao Chen[1,*], Lin Zhang[1], Hao Zhou[1], Wei Li[1], Bong Kwon Son[1], and Chuan Seng Tan[1,*]

[1] School of Electrical and Electronic Engineering, Nanyang Technological University, 50 Nanyang Avenue, 639798 Singapore.

Email: chenqm@ntu.edu.sg; tancs@ntu.edu.sg

Abstract

A direct band gap type-I $Ge_{0.75}Sn_{0.25}/Ge_{0.682}Sn_{0.158}Si_{0.16}$ QD heterostructure is proposed for mid-IR light sources. The effects of strain and composition are theoretically investigated to optimize the band offset of the direct band gap GeSn QDs. It is found that the introduction of tensile strain and Si incorporation in the barrier layers are effective to increase the band offset in the conduction band. Besides, the band offset is expected to increase with the increase of Sn composition in QDs and the size of QDs.

Keywords: GeSn QD, mid-IR light source

1. Introduction

Si photonics has been widely regarded as a key technology for future generation of data communication and computation systems with low-power-consumption and high-performance. Great progress has been made in recent years through the investigation of group IV materials, such as Ge based modulators [1], photodetectors [2] and lasers [3,4]. However, Si-based light source remains as one of the major bottlenecks in the development of Si photonics due to the indirect band gap nature of Si. Ge has been a promising material to resolve the bottleneck due to its pseudo-direct band gap and compatibility with Si complementary metal oxide semiconductor (CMOS) processing. It has been theoretically predicted that GeSn alloy with a Sn content of 6-11% [5–10] or 1.4-2.0% biaxial tensile strain [11–13] can convert Ge into a direct band gap semiconductor. More interestingly, light emitters can be improved by the introduction of heterostructures and quantum confinement effects (QCEs). Besides, GeSn QDs are easier to realize even at higher Sn content and are more robust to defects [14] than bulk materials and quantum well structures, thus improving the overall optical gain. In addition to low threshold current density, it has been shown that QDs-based lasers can also offer reduced temperature sensitivity [15,16]. A few groups have demonstrated the growth of GeSn QDs on different matrixes, including SiO_2 matrix [17], bare [18] and patterned Si substrate [19,20]. However, there is no systematic theoretical investigation of the QCE of GeSn QDs/GeSnSi heterostructures with different composition and strain in the QDs and barriers.

In this work, we consider a model of GeSn QD buried in GeSnSi barrier which constructs a direct band gap type-I heterostructure to confine both electrons and holes in the QDs. The effect of strain, composition and quantum confinement on GeSn QD are carefully investigated by varying the Sn composition of GeSn QDs with different size, the strain and composition of GeSnSi barrier.

2. Proposed Method

Spherical cap GeSn QDs with GeSnSi barrier layers on relaxed (001) GeSn buffer is theoretically investigated (Fig. 1a). Strain relaxed GeSn buffer layer, which is acted as virtual substrates (VS) for GeSn QD/GeSnSi heterostructure, is grown on (001) Ge/Si or (001) Si substrate. The GeSnSi barrier layers are grown pseudomorphically on the GeSn buffer layer. Since the in-plane lattice constant of pseudomorphic GeSnSi barrier layers equals to that

of GeSn buffer layer, the strain in GeSn QDs is introduced by the lattice mismatch between GeSn QDs layer and GeSn buffer layer which is given by $\varepsilon=(a_{VS}-a_{GeSn})/a_{GeSn}$, where a_{VS} and a_{GeSn} are relaxed lattice constant of GeSn VS layer and GeSn QD layer, respectively. The shape and size of the QD are based on the Ge QDs we have grown previously [21]. Except for the band gap, the most composition-dependent parameters of GeSn and GeSnSi materials are calculated by linear interpolation of Si, Ge and α-Sn. The parameters of Si, Ge and α-Sn for the calculation is from reference [22]. The band gap of GeSn and GeSnSi can be expressed with bowing parameter as [23]:

$$E_{g,\eta}(Ge_{1-x}Sn_x) = xE_{g,\eta}(Sn) + (1-x)E_{g,\eta}(Ge) - x(1-x)b_{\eta,GeSn} \quad (1)$$

$$E_{g,\eta}(Ge_{1-y-x}Sn_xSi_y) = xE_{g,\eta}(Sn) + yE_{g,\eta}(Si) + (1-y-x)E_{g,\eta}(Ge) - yxb_{\eta,SiSn} - y(1-y-x)b_{\eta,SiGe} - x(1-y-x)b_{\eta,GeSn} \quad (2)$$

where $b_{\eta,SiGe}$, $b_{\eta,GeSn}$ and $b_{\eta,SiSn}$ (η=Γ, L refers to different conduction valleys) are the band gap bowing parameters of SiGe, GeSn and SiSn alloys, respectively. The band gap bowing parameters used for this calculation are listed in Table I. For GeSn alloys, the bowing parameters, especially Γ-valley band gap bowing parameter, were explored both experimentally and theoretically. However, the GeSn bowing parameters reported are not consistent in different literature. The discrepancy is mainly due to temperature, strain and Burstein-Moss effects [24]. The GeSn bowing parameter from strained GeSn at room temperature ($b_{\Gamma,GeSn}$: 1.94 eV [25], 1.95 eV [26], 1.8±0.2 eV [27], 2.3 eV [28], 2.4 eV [29] and 2.42 eV [30]) are lower than that from unstrained GeSn at low temperature ($b_{\Gamma,GeSn}$: 2.8 eV [31], 2.84 eV [28], 2.87 eV [32], 2.9 eV [33], 3.02 eV [24] and 3.1 eV [34]). In addition, some groups suggested composition-dependent bowing parameters [35]. In our case, the GeSn bowing parameter from strained GeSn at room temperature is reasonable since the GeSn QDs/GeSnSi calculated is for light sources at room temperature. The SiGe bowing parameters are small and consistent. Different from SiGe and GeSn bowing parameters, the uncertainty of Γ-valley band gap bowing parameters of SiSn alloys from literature is large. For experimental studies, the deduced SiSn bowing parameters are 13.2 eV [36], -21 eV [37] and 24±2 eV [38]. The theoretical SiSn bowing parameters are 3.92 eV [39] and -5.95 eV [40]. In this work, the SiSn bowing parameter is taken from the value deduced from spectroscopic ellipsometer of GeSnSi which is between the minimum value of -21 eV and the maximum value of 24 eV. It needs more works to find out the reason for the discrepancy of SiSn bowing parameters in the future.

Table I Γ- and L-valley band gap bowing parameters of SiGe, GeSn and SiSn alloys. [25,36,41,42]

Parameter @ 300 K	**SiGe**	**GeSn**	**SiSn**
b_Γ (eV)	0.21	1.94	13.2
b_L (eV)	0.169	1.23	0.925

The band alignment is evaluated by model-solid theory [43]. The potential profile with strain and the ground states of GeSn/GeSnSi QDs is calculated by deformation potential theory and single-band effective mass approach [44]:

$$H_\eta \Psi_\eta(\boldsymbol{r}) = E_\eta \Psi_\eta(\boldsymbol{r}) \quad (3)$$

where H_η, Ψ_η and E_η (η=Γ, L, LH and HH) refer to the Hamiltonian, wavefunction and eigenenergy of different conduction and valence bands, respectively. **r** is the three-dimension (3D) coordinate vector. For Γ-conduction band, the single-band Hamiltonian of the envelope function with strain effect can be expressed as follows:

$$H_\Gamma = -\frac{\hbar^2}{2}\nabla\frac{1}{m_c{}^*}\nabla + V_c(\boldsymbol{r}) + V_{c\varepsilon}(\boldsymbol{r}) \quad (4)$$

$$V_{ce} = a_c(\varepsilon_{xx} + \varepsilon_{yy} + \varepsilon_{zz}) \quad (5)$$

where m_c^* is the effective mass. V_c is the intrinsic band profile of the Γ-conduction band and $V_{c\varepsilon}$ is strain

induced band edge shift. a_c is the deformation potential of the Γ-conduction band. $\varepsilon_{xx}=\varepsilon_{yy}=(a_{VS} - a_{GeSn(Si)})/a_{GeSn(Si)}$ is the in-plane strain of GeSn QDs (GeSnSi barrier layers), $\varepsilon_{zz}=(-2c_{12}/c_{11})\varepsilon_{xx}$ is the strain in (001) direction. a_{GeSnSi} is the strain relaxed lattice constant of GeSnSi barrier layers. c_{12} and c_{11} are the elastic constants. For L-conduction band, the Hamiltonian with strain effect under the effective-mass approximation can be written as:

$$H_L = -\frac{\hbar^2}{2}\nabla\cdot\overleftrightarrow{\boldsymbol{W}}\cdot\nabla + V_L(\boldsymbol{r}) + V_{L\varepsilon}(\boldsymbol{r}) \quad (6)$$

$$V_{L\varepsilon} = a_L(\varepsilon_{xx} + \varepsilon_{yy} + \varepsilon_{zz}) \quad (7)$$

$$\overleftrightarrow{\boldsymbol{W}} = \begin{bmatrix} \frac{1}{3}(\frac{1}{m_t^L} + \frac{2}{m_l^L}) & 0 & \frac{\sqrt{2}}{3}(\frac{1}{m_t^L} - \frac{1}{m_l^L}) \\ 0 & \frac{1}{m_t^L} & 0 \\ \frac{\sqrt{2}}{3}(\frac{1}{m_t^L} - \frac{1}{m_l^L}) & 0 & \frac{1}{3}(\frac{2}{m_t^L} + \frac{1}{m_l^L}) \end{bmatrix} \quad (8)$$

where $\overleftrightarrow{\boldsymbol{W}}$ is the inverse effective mass. V_L and $V_{c\varepsilon}$ are the intrinsic band edge and strain induced band edge shift of the L conduction-band, respectively. a_L is the deformation potential of L-conduction band. m_t^L and m_l^L are the longitudinal and transverse effective mass along the [111] direction. For light hole and heavy hole bands, the Hamiltonians can be given by:

$$H_{lh} = \frac{\hbar^2}{2}\left(\frac{\partial}{\partial x}\frac{1}{m_t}\frac{\partial}{\partial x} + \frac{\partial}{\partial y}\frac{1}{m_t}\frac{\partial}{\partial y} + \frac{\partial}{\partial z}\frac{1}{m_z}\frac{\partial}{\partial z}\right) + V_{lh}(\boldsymbol{r}) + V_{lh\varepsilon}(\boldsymbol{r}) \quad (9)$$

$$H_{hh} = \frac{\hbar^2}{2}\left(\frac{\partial}{\partial x}\frac{1}{m_{thh}}\frac{\partial}{\partial x} + \frac{\partial}{\partial y}\frac{1}{m_{thh}}\frac{\partial}{\partial y} + \frac{\partial}{\partial z}\frac{1}{m_{zhh}}\frac{\partial}{\partial z}\right) + V_{hh}(\boldsymbol{r}) + V_{hh\varepsilon}(\boldsymbol{r}) \quad (10)$$

$$V_{lh\varepsilon} = -P_\varepsilon + \frac{1}{2}(Q_\varepsilon - \Delta + \sqrt{\Delta^2 + 2Q_\varepsilon\Delta + 9Q_\varepsilon^2}) \quad (11)$$

$$V_{hh\varepsilon} = -P_\varepsilon - Q_\varepsilon \quad (12)$$

$$P_\varepsilon = -a_v(\varepsilon_{xx} + \varepsilon_{yy} + \varepsilon_{zz}) \quad (13)$$

$$Q_\varepsilon = -\frac{b}{2}(\varepsilon_{xx} + \varepsilon_{yy} - 2\varepsilon_{zz}) \quad (14)$$

where m_t and m_z refer to the transverse and longitudinal effective mass of light hole band, respectively. m_{thh} and m_{zhh} are the transverse and longitudinal effective mass of heavy hole band, respectively. V_{lh} and $V_{lh\varepsilon}$ are the intrinsic band edge and strain induced band edge shift of the light hole band, respectively. V_{hh} and $V_{hh\varepsilon}$ are the intrinsic band edge and strain induced band edge shift of the heavy hole band, respectively. Δ is the spin-orbital splitting of the valence band. a_v and b are the deformation potentials of the Γ valence band.

3. Results and Discussion

The lattice mismatch between GeSn QDs layer and GeSn VS layer can be tuned by changing the Sn content of GeSn VS layer (Fig. 1b). Considering experimental realization of GeSn QDs by widely used Stranski-Krastanov (SK) growth mode, the minimum lattice mismatch required to form GeSn SK QDs with different Sn concentration is labeled by black dashed lines in Figure 1b. Due to the lack of study on the growth of GeSn QDs/GeSnSi structures, the critical lattice mismatch to form SK QDs is taken from SiGe QDs/Si structure [45] as a reference. GeSn SK QDs with low Sn contents tend to be tensilly strained while GeSn SK QDs with high Sn contents tend to be compressively strained. In addition to SK QDs, to grow GeSn QDs with small lattice mismatch or matched lattice constants, lattice-matched techniques [46], such as droplet epitaxy (DE) method or top-down approaches based on lithography and etching of quantum wells, need to be utilized in the future.

The band structure of a 3D spherical cap $Ge_{0.75}Sn_{0.25}$ QD with a diameter of 100 nm and a height of 20 nm was studied. The barrier layers are

$Ge_{0.682}Sn_{0.158}Si_{0.16}$ with a biaxial tensile strain of 0.5% which can be induced by the lattice mismatch between the GeSnSi barrier layer and GeSn buffer. Fig. 1(c) shows the 1D potential profile of the GeSn QD along [001] direction at 300 K and the ground levels of bands are represented by the dashed lines. The inset shows the squared electron ground state wavefunction. Both the energies of conduction and valence bands in GeSn QD are lower than those in barrier layers, indicating a type-I band alignment. The band offset of Γ-conduction band is as high as 101 meV which is almost 4 times of that of thermal energy at room temperature (k_BT~25 meV) which will suppress the thermally activated carrier transfer from GeSn QD to barrier layers and increase the wavefunction overlaps of electrons and holes, thus causing an increase in light emission at room temperature. The Γ-electron wavefunction is confined in GeSn QD as shown in the inset. Besides, the Γ-conduction band in GeSn QD lies 50 meV lower than L-conduction band, indicating the direct band gap of the GeSn QD. Since the effective mass of Γ-conduction valley is smaller than that of the L-conduction valley, the energy lift of Γ-conduction valley is faster than that of L-conduction valley by QCE, resulting in the reduction of the directness and band offset. However, even considering the QCE, the ground level of Γ-conduction band is 46 meV lower than the ground level of L. The QCE will reduce the band offset from 101 to 81 meV. The transition energy from the ground state of Γ-conduction band to the ground state of heavy hole band is 241 meV. The split of the heavy hole and the light hole band is due to the compressive strain in the GeSn QD.

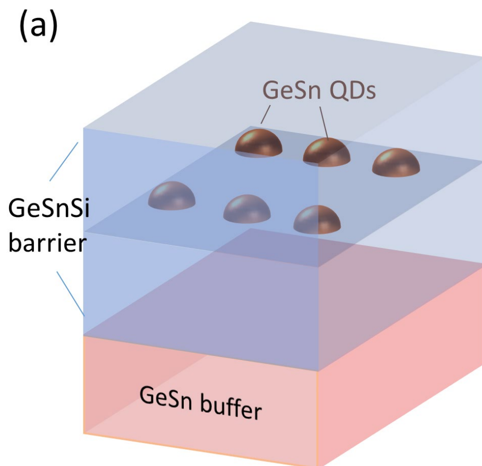

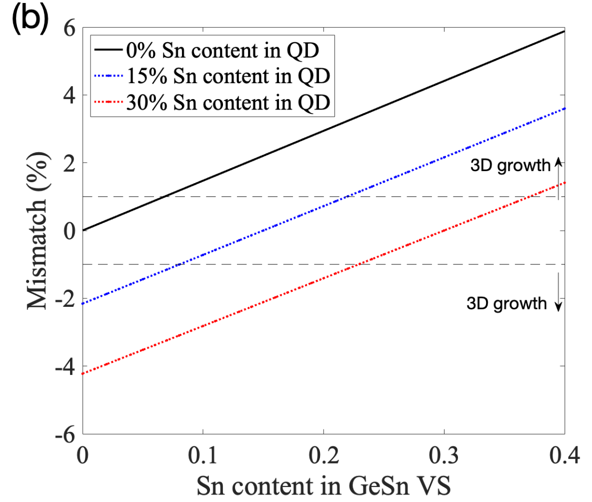

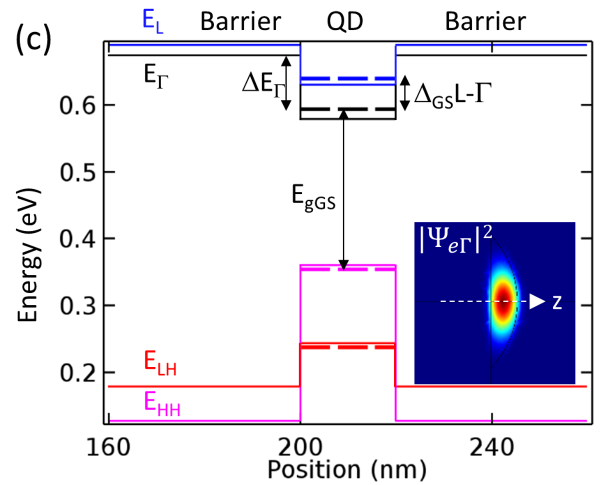

Figure 1 (a) Schematic of the GeSn/GeSnSi QD structure. (b) Lattice mismatch between the GeSn QDs layer with different Sn content and the GeSn VS layer as a function of Sn content in GeSn VS layer. (c) Potential profile of a 3D spherical cap $Ge_{0.75}Sn_{0.25}$ QD which is buried in $Ge_{0.682}Sn_{0.158}Si_{0.16}$ barrier layers with a biaxial strain of 0.5%. The inserted figure shows the squared *Γ* electrons' wavefunction.

In order to optimize the GeSnSi barrier to achieve the highest band offset, the effect of Sn and Si compositions on the band offset of $Ge_{0.84}Sn_{0.16}$ QD buried in strain-free GeSnSi barrier without QCE is calculated (Fig. 2a). Warmer color indicates larger band offset and the contour lines of the band offset is represented by black lines. The value of the band offset is labeled by black numbers. Three bold lines denoted as boundaries of the area with direct band gap type-I GeSn/GeSnSi. The bold black line is contour line of band offset with a value of 0 and the arrows show the gradient vectors. The pink bold line

and red bold line are the boundaries of direct band gap GeSn active layer and the region with $E_{L,barrier}$-$E_{\Gamma,QD}$>0, respectively. According to Fig. 2(a), the area defined by the black bold line and pink bold line satisfies the condition of direct gap type-I GeSn QD. Increasing the Si content and decreasing the Sn content can increase the band offset significantly. The highest band offset of direct band gap $Ge_{0.84}Sn_{0.16}$/GeSnSi that can be achieved is as large as 108 meV when the Si and Sn content in barriers are 17.2% and 15%, respectively. The directness of GeSn active layer was also calculated as shown in Fig. 2(b). The boundary of the direct band gap GeSn is labeled as the pink bold line. Increasing Sn content and decreasing Si content in barrier layer increase the directness of GeSn active layer. Without Si, $Ge_{0.897}Sn_{0.103}$ barrier layer can convert $Ge_{0.84}Sn_{0.16}$ active layer to direct band gap material with a directness of 0 eV. When the ΔSn/ΔSi ratio in the barrier is 0.27, the directness of GeSn active layer remains constant.

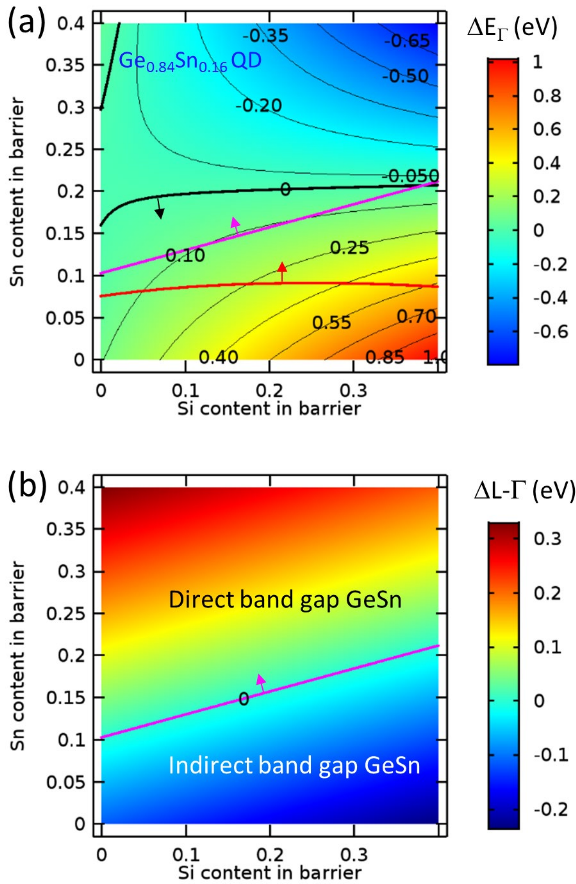

Figure 2 $Ge_{0.84}Sn_{0.16}$/GeSnSi QDs: (a) Band offset at Γ point, ΔE_Γ and (b) the directness of $Ge_{0.84}Sn_{0.16}$ QDs, ΔL-Γ as functions of Sn and Si compositions of relaxed barrier layers without QCE.

Besides the Sn and Si compositions in barrier layers, the strain in barrier layer, which is induced by the lattice mismatch between the GeSnSi barrier layer and GeSn buffer layer, also has a profound influence on the band offset. Fig. 3(a) shows the band offset of $Ge_{0.84}Sn_{0.16}$/GeSnSi with 0.5% biaxial tensile strain in the barrier layer. Comparing Fig. 3(a) with Fig. 2(a), the strain in the barrier almost does not change the distribution of the band offset, but it makes the direct band gap boundary line lower, indicating that tensile strain in barrier makes the directness of GeSn active layer larger. Thus, when the GeSn active layer remains direct band gap, the band offset can increase up to 196 meV with Si content of 23.5% and Sn content of 13.3%, respectively, in the barrier. Fig. 3(b) shows the maximum band offset achievable in the barrier when the strain in barrier varies from compressive strain to tensile strain. Tensile strain increases band offset while compressive strain decreases the band offset. A 0.75% biaxial tensile strain in the barrier can achieve as high as 250 meV band offset which is 10 times of thermal energy at room temperature. Therefore, it can be concluded that the introduction of tensile strain into barrier layers is an effective way to increase the band offset.

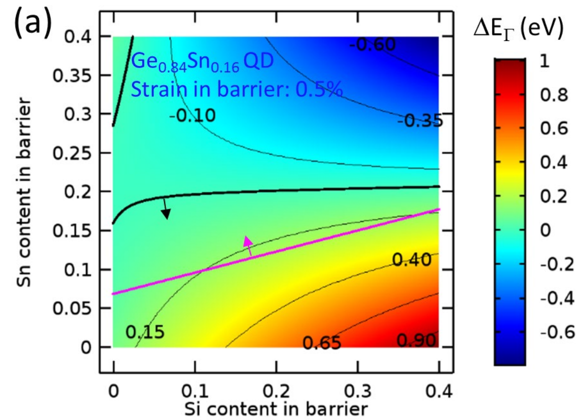

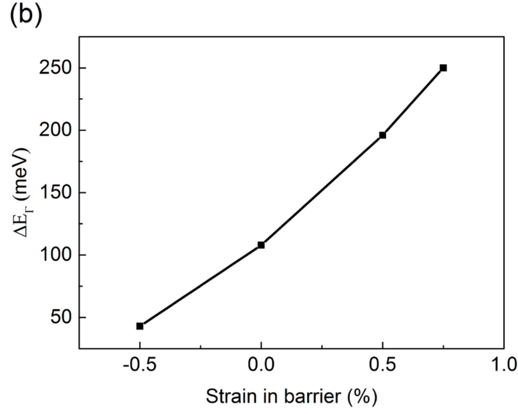

Figure 3 (a) Band offset at Γ point, ΔE_Γ as functions of Sn and Si compositions of barrier layers with 0.5% biaxial strain without QCE. (b) ΔE_Γ vs. strain of barrier without QCE.

Furthermore, the properties of GeSn QDs, such as the size and Sn content of QDs, can be critical for the band offset and directness. Fig. 4(a) shows the band offset of GeSn/GeSnSi QDs whose Sn content increases to 25%. Compared to GeSn QDs with Sn content of 16% shown in Fig. 2(a), the contour line of the directness (the pink bold line) remains almost the same while the band offset increases. The reason that the directness is almost the same is that the reduction effect of Sn composition on the band gaps of GeSn alloys is compensated by the introduced compressive strain in the QDs. The maximum band offset of direct gap GeSn/GeSnSi QD increases from 108 to 135 meV when the Sn content in QD increases from 16 to 25%. The maximum band offset of $Ge_{0.75}Sn_{0.25}$/GeSnSi QDs is achieved by the $GeSn_{0.146}Si_{0.172}$ barrier layer. The band offset of GeSn/GeSnSi with different Sn content in GeSn QD is shown in Fig. 4(b). The band offset increases to nearly 3 times when the Sn content in GeSn QD varies from 5 to 25%.

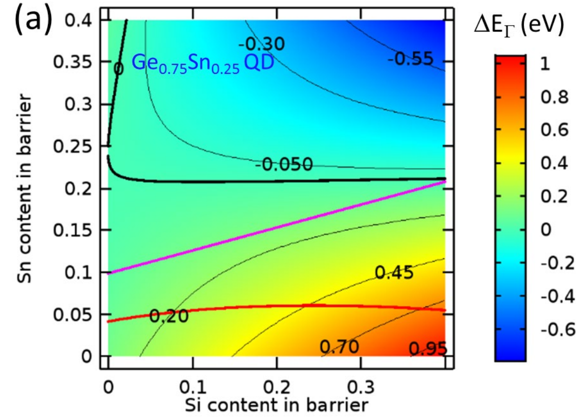

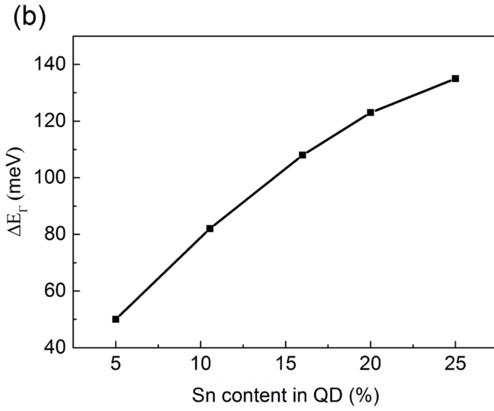

Figure 4 (a) Band offset at Γ point, ΔE_Γ of $Ge_{0.75}Sn_{0.25}$/GeSnSi QD as functions of Sn and Si compositions of relaxed barrier layers without QCE. (b) ΔE_Γ vs. Sn content in GeSn QD without QCE

The size effect is one of the most important features of QDs. According to above results, in order to achieve direct band gap GeSn/GeSnSi QDs with high band offset, tensile strain in the barrier with proper Si and Sn contents as well as high Sn content in QD are required. Here the GeSn QD buried in $Ge_{0.682}Sn_{0.158}Si_{0.16}$ barrier layers with 0.5% tensile strain was employed to investigate the size effect. The reason to choose $Ge_{0.682}Sn_{0.158}Si_{0.16}$ as the barrier layer is to achieve the highest band offset when the directness of GeSn QD is 50 meV without QCE. The band offset of $Ge_{0.75}Sn_{0.25}$/GeSnSi QD is shown in Fig. 5(a) and the pink bold line represents the contour line of directness with a value of 50 meV. Then, the QD with a diameter varies from 15 to 100 nm (diameter/height=5) is utilized to investigate the size effect on the band offset, the directness and the transition energy from ground states. The range of the size is from the Ge QDs we grew previously [47]. As shown in Fig. 5(b), the band offset is reduced as the

size is decreased due to QCE. For the QD with a Sn content of 30%, when the diameter of the QD increases from 15 to 100 nm, the band offset increases from 3 to 80 meV. For the QD with the smallest diameter of 15 nm, there is almost no confinement for electrons. Considering QCE, for the largest QD with the size of 100 nm diameter by 20 nm height, when the Sn content in QD varies from 5 to 30%, the band offset increases from 25 to 80 meV. Besides, the size effect on the directness of QDs is shown in Fig. 5(c). QCE reduces the directness of GeSn QD. For GeSn QD with Sn content of 30%, when the diameter of the QD decreases from 100 to 15 nm, the directness of the QD decrease from 47 (50 meV without QCE) to 18 meV. Since the effective mass of Γ-conduction valley is less than that of L-conduction valley, the lift of Γ-conduction valley by QCE is faster than L-conduction valley, thus reducing the directness. Compared to relaxed GeSn bulk, the effect of Sn content in the QD on the directness is not obvious due to the compressive strain in the QD. Fig. 5(d) shows the interband transition energy between ground states of GeSn QDs. For GeSn QD with Sn content of 30%, when the diameter of the QD increases from 15 to 100 nm, the transition energy decreases from 0.375 to 0.175 eV, which is in the range of mid-infrared radiation. For GeSn QD with the size of 100 nm diameter by 20 nm height, the Sn content in the QD is varied from 5 to 30%. It is observed that the transition energy decreases from 0.402 to 0.175 eV due to the reduction effect of Sn on the band gap of GeSn alloys. The highest transition energy is 0.494 eV which is from the smallest $Ge_{0.8}Sn_{0.2}$ QD with a diameter of 15 nm and a height of 3 nm. When the Sn content is higher than 15%, the interband transition is from ground states of the Γ-conduction valley to the heavy hole band. When the Sn content is less than 10%, the interband transition is from the ground state of the Γ-conduction valley to that of the light hole band. The phenomenon is due to the strain conversion from tensile strain to compressive strain in the GeSn QD with the increasing of Sn content in the QD. Besides, the built-in strain of GeSn QDs will change the polarization of light from GeSn QDs which has been theoretically investigated by GeSn /GeSnSi quantum well recently [24]. In many applications, non-polarization is preferred. In the future work, tuning the strain and composition of GeSn QDs/GeSnSi to achieve both high band offset and insensitive light polarization will be investigated. Compared with GeSn/GeSnSi quantum wells [48], GeSn/GeSnSi QDs have the advantages of robust to defects, temperature insensitivity and tunable band gap by QCE or Sn compositions, but they also suffer from the same issue of reduced directness of band gaps with decreased sizes.

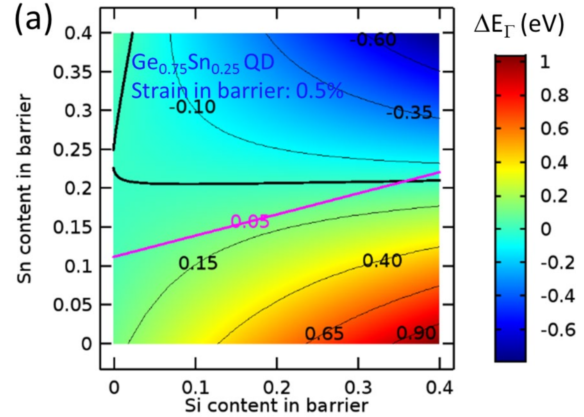

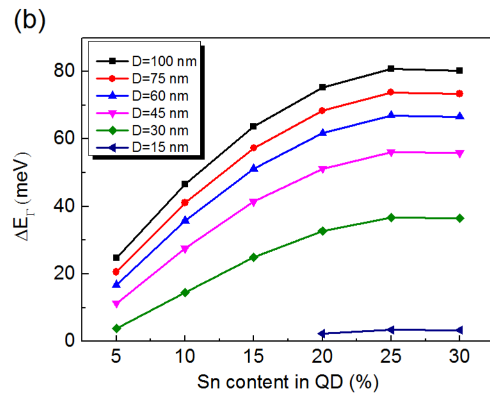

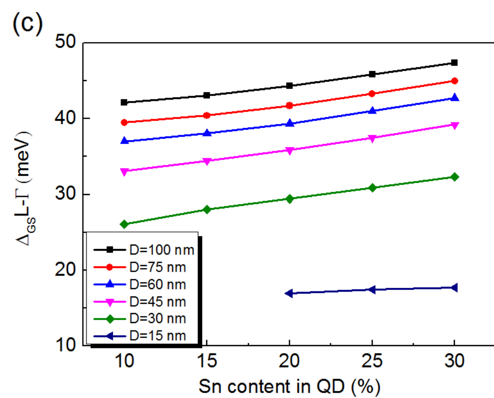

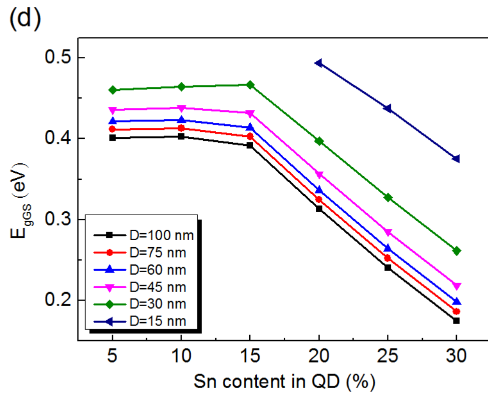

Figure 5 (a) Band offset at Γ point, ΔE_{Γ} of $Ge_{0.75}Sn_{0.25}$ QD as functions of Sn and Si compositions of barrier layers with 0.5% biaxial strain without QCE. (b) Band offset at Γ point ΔE_{Γ}, (c) directness ΔL-Γ and (d) interband transition energy from ground states E_{gGS} of GeSn/$Ge_{0.682}Sn_{0.158}Si_{0.16}$ QD with different sizes as functions of Sn composition in QDs.

4. Conclusion

A direct band gap type-I $Ge_{0.75}Sn_{0.25}/Ge_{0.682}Sn_{0.158}Si_{0.16}$ QD heterostructure with band offset of 81 meV and directness of 46 meV is proposed. Several key factors, including composition in barrier layers and QDs, strain in barrier layers and size of QDs, are investigated to optimize the band offset of direct band gap GeSn QD. Besides increasing the Si content and decreasing the Sn content in the barriers, tensile strain can increase the band offset significantly. For QDs, the band offset is expected to increase with the increase of the Sn composition in QDs and the sizes of QDs. The transition energy from the ground states can vary from 0.175 to 0.494 eV by different size and Sn content in GeSn QDs. This work indicates that GeSn QD/GeSnSi is a promising route toward CMOS compatible mid-IR light source for integrated photonics.

Acknowledgments

The authors would like to thank the financial support from the National Research Foundation of Singapore under the Competitive Research Program (NRF–CRP19–2017–01).

References

[1] Liu J, Beals M, Pomerene A, Bernardis S, Sun R, Cheng J, Kimerling L C and Michel J 2008 Waveguide-integrated, ultralow-energy GeSi electro-absorption modulators *Nat. Photonics* **2** 433–7

[2] Michel J, Liu J and Kimerling L C 2010 High-performance Ge-on-Si photodetectors *Nat. Photonics* **4** 527–34

[3] Camacho-aguilera R E, Cai Y, Patel N, Bessette J T, Romagnoli M, Kimerling L C and Michel J 2012 An electrically pumped germanium laser **20** 11316–20

[4] Bao S, Kim D, Onwukaeme C, Gupta S, Saraswat K, Lee K H, Kim Y, Min D, Jung Y, Qiu H, Wang H, Fitzgerald E A, Tan C S and Nam D 2017 Low-threshold optically pumped lasing in highly strained germanium nanowires *Nat. Commun.* **8** 1–7

[5] Lu Low K, Yang Y, Han G, Fan W and Yeo Y-C 2012 Electronic band structure and effective mass parameters of Ge 1-x Sn x alloys *J. Appl. Phys.* **112** 103715

[6] Gupta S, Magyari-Köpe B, Nishi Y and Saraswat K C 2013 Achieving direct band gap in germanium through integration of Sn alloying and external strain *J. Appl. Phys.* **113** 073707

[7] Tonkikh A A, Eisenschmidt C, Talalaev V G, Zakharov N D, Schilling J, Schmidt G and Werner P 2013 Pseudomorphic GeSn/Ge(001) quantum wells: Examining indirect band gap bowing *Appl. Phys. Lett.* **103** 032106

[8] Dutt B, Lin H, Sukhdeo D S, Vulovic B M, Gupta S, Nam D, Saraswat K C and Harris J S 2013 Theoretical analysis of GeSn alloys as a gain medium for a Si-compatible laser *IEEE J. Sel. Top. Quantum Electron.* **19** 1502706

[9] Kotlyar R, Avci U E, Cea S, Rios R, Linton T D, Kuhn K J and Young I A 2013 Bandgap engineering of group IV materials for complementary n and p tunneling field effect transistors *Appl. Phys. Lett.* **102** 113106

[10] Wirths S, Geiger R, Von Den Driesch N, Mussler G, Stoica T, Mantl S, Ikonic Z, Luysberg M, Chiussi S, Hartmann J M, Sigg H, Faist J, Buca D, Gruetzmacher D and Grützmacher D 2015 Lasing in direct-bandgap GeSn alloy grown on Si *Nat. Photonics* **9** 88–92

[11] Tahini H, Chroneos A, Grimes R W, Schwingenschlögl U and Dimoulas A 2012 Strain-induced changes to the electronic structure of germanium *J. Phys. Condens. Matter* **24** 195802

[12] El Kurdi M, Prost M, Ghrib A, Sauvage S, Checoury X, Beaudoin G, Sagnes I, Picardi G, Ossikovski R and Boucaud P 2016 Direct Band Gap Germanium Microdisks Obtained with Silicon Nitride Stressor Layers *ACS Photonics* **3** 443–8

[13] Fischetti M V. and Laux S E 1996 Band structure, deformation potentials, and carrier mobility in strained Si Ge, and SiGe alloys *J. Appl. Phys.* **80** 2234–52

[14] Liu A Y, Srinivasan S, Norman J, Gossard A C and Bowers J E 2015 Quantum dot lasers for silicon photonics [Invited] *Photonics Res.* **3** B1

[15] Chen S, Li W, Wu J, Jiang Q, Tang M, Shutts S, Elliott S N, Sobiesierski A, Seeds A J, Ross I, Smowton P M and Liu H 2016 Electrically pumped continuous-wave III-V quantum dot lasers on silicon *Nat. Photonics* **10** 307–11

[16] Grundmann M, Christen J, Ledentsov N N, Böhrer J, Bimberg D, Ruvimov S S, Werner P, Richter U, Gösele U, Heydenreich J, Ustinov V M, Egorov A Y, Zhukov A E, Kop'Ev P S and Alferov Z I 1995 Ultranarrow luminescence lines from single quantum dots *Phys. Rev. Lett.* **74** 4043–6

[17] Nakamura Y, Masada A and Ichikawa M 2007 Quantum-confinement effect in individual Ge 1- x Sn x quantum dots on Si (111) substrates covered with ultrathin Si O 2 films using scanning tunneling spectroscopy *Appl. Phys. Lett.* **91** 13109

[18] Naruse N, Mera Y, Nakamura Y, Ichikawa M and Maeda K 2009 Fourier-transform photoabsorption spectroscopy of quantum-confinement effects in individual GeSn nanodots *Appl. Phys. Lett.* **94** 2007–10

[19] Schlykow V, Zaumseil P, Schubert M A, Skibitzki O, Yamamoto Y, Klesse W M, Hou Y, Virgilio M, De Seta M, Di Gaspare L, Schroeder T and Capellini G 2018 Photoluminescence from GeSn nano-heterostructures *Nanotechnology* **29** 415702

[20] Di Bartolomeo A, Passacantando M, Niu G, Schlykow V, Lupina G, Giubileo F and Schroeder T 2016 Observation of field emission from GeSn nanoparticles epitaxially grown on silicon nanopillar arrays *Nanotechnology* **27** 485707

[21] Chen Q, Song Y, Wang K, Yue L, Lu P, Li Y, Gong Q and Wang S 2015 A new route toward light emission from Ge: Tensile-strained quantum dots *Nanoscale* **7** 8725–30

[22] Chang G E, Chang S W and Chuang S L 2010 Strain-balanced GezSn1-z-SixGeySn1-x-ymultiple-quantum-well lasers *IEEE J. Quantum Electron.* **46** 1813–20

[23] D'Costa V R, Cook C S, Menéndez J, Tolle J, Kouvetakis J and Zollner S 2006 Transferability of optical bowing parameters between binary and ternary group-IV alloys *Solid State Commun.* **138** 309–13

[24] Polak M P, Scharoch P and Kudrawiec R 2017 The electronic band structure of Ge 1− x Sn x in the full composition range: indirect, direct, and inverted gaps regimes, band offsets, and the Burstein–Moss effect *J. Phys. D. Appl. Phys.* **50** 195103

[25] D'costa V R, Cook C S, Birdwell A G, Littler C L, Canonico M, Zollner S, Kouvetakis J and Menéndez J 2006 Optical critical points of thin-film Ge 1- y Sn y alloys: a comparative Ge 1- y Sn y/ Ge 1- x Si x study *Phys. Rev. B* **73** 125207

[26] Ryu M Y, Harris T R, Yeo Y K, Beeler R T and Kouvetakis J 2013 Temperature-dependent photoluminescence of Ge/Si and Ge 1-ySny/Si, indicating possible indirect-to-direct bandgap transition at lower Sn content *Appl. Phys. Lett.* **102** 1–5

[27] Zelazna K, Polak M P, Scharoch P, Serafinczuk J, Gladysiewicz M, Misiewicz J, Dekoster J and Kudrawiec R 2015 Electronic band structure of compressively strained Ge 1−x Sn x with x < 0.11 studied by contactless electroreflectance *Appl. Phys. Lett.* **106** 142102

[28] Pérez Ladrón de Guevara H, Rodríguez A G, Navarro-Contreras H and Vidal M A 2007 Nonlinear behavior of the energy gap in Ge1−xSnx alloys at 4K *Appl. Phys. Lett.* **91** 161909

[29] Dybała F, Żelazna K, Maczko H, Gladysiewicz M, Misiewicz J, Kudrawiec R, Lin H, Chen R, Shang C, Huo Y, Kamins T I and Harris J S 2016 Electromodulation spectroscopy of direct optical transitions in Ge 1−x Sn x layers under hydrostatic pressure and built-in strain *J. Appl. Phys.* **119** 215703

[30] Lin H, Chen R, Lu W, Huo Y, Kamins T I and Harris J S 2012 Investigation of the direct band gaps in Ge 1−x Sn x alloys with strain control by photoreflectance spectroscopy *Appl. Phys. Lett.* **100** 102109

[31] He G and Atwater H A 1997 Interband transitions in Sn x Ge 1- x alloys *Phys. Rev. Lett.* **79** 1937

[32] Yin W-J, Gong X-G and Wei S-H 2008 Origin of the unusually large band-gap bowing and the breakdown of the band-edge distribution rule in the Sn x Ge 1- x alloys *Phys. Rev. B* **78** 161203

[33] Chibane Y and Ferhat M 2010 Electronic structure of SnxGe1−x alloys for small Sn compositions: Unusual structural and electronic properties *J. Appl. Phys.* **107** 053512

[34] Eckhardt C, Hummer K and Kresse G 2014 Indirect-to-direct gap transition in strained and unstrained Sn x Ge 1- x alloys *Phys. Rev. B* **89** 165201

[35] Gallagher J D, Senaratne C L, Kouvetakis J and Menéndez J 2014 Compositional dependence of the bowing parameter for the direct and indirect band gaps in Ge 1 − y Sn y alloys *Appl. Phys. Lett.* **105** 142102

[36] D'Costa V R, Fang Y-Y, Tolle J, Kouvetakis J and Menéndez J 2009 Tunable Optical Gap at a Fixed Lattice Constant in Group-IV Semiconductor Alloys *Phys. Rev. Lett.* **102** 107403

[37] Lin H, Chen R, Lu W, Huo Y, Kamins T I and Harris J S 2012 Structural and optical characterization of Si x Ge 1−x − y Sn y alloys grown by molecular beam epitaxy *Appl. Phys. Lett.* **100** 141908

[38] Wendav T, Fischer I A, Montanari M, Zoellner M H, Klesse W, Capellini G, von den Driesch N,

Oehme M, Buca D, Busch K and Schulze J 2016 Compositional dependence of the band-gap of Ge 1− x − y Si x Sn y alloys *Appl. Phys. Lett.* **108** 242104

[39] Moontragoon P, Soref R A and Ikonic Z 2012 The direct and indirect bandgaps of unstrained Si x Ge 1−x−y Sn y and their photonic device applications *J. Appl. Phys.* **112** 073106

[40] Sant S and Schenk A 2014 Pseudopotential calculations of strained-GeSn/SiGeSn hetero-structures *Appl. Phys. Lett.* **105** 162101

[41] Moontragoon P, Ikonić Z and Harrison P 2007 Band structure calculations of Si-Ge-Sn alloys: Achieving direct band gap materials *Semicond. Sci. Technol.* **22** 742–8

[42] D'Costa V R, Cook C S, Menéndez J, Tolle J, Kouvetakis J and Zollner S 2006 Transferability of optical bowing parameters between binary and ternary group-IV alloys *Solid State Commun.* **138** 309–13

[43] Van de Walle C G 1989 Band lineups and deformation potentials in the model-solid theory *Phys. Rev. B* **39** 1871–83

[44] Chuang S L 2012 *Physics of photonic devices* vol 80 (John Wiley & Sons)

[45] Brunner K 2001 Si/Ge nanostructures *Reports Prog. Phys.* **65** 27

[46] Gurioli M, Wang Z, Rastelli A, Kuroda T and Sanguinetti S 2019 Droplet epitaxy of semiconductor nanostructures for quantum photonic devices *Nat. Mater.* **18** 799–810

[47] Zhang Z P, Song Y X, Chen Q M, Wu X Y, Zhu Z Y S, Zhang L Y, Li Y Y and Wang S M 2017 Growth mode of tensile-strained Ge quantum dots grown by molecular beam epitaxy *J. Phys. D. Appl. Phys.* **50** 465301

[48] Fujisawa T and Saitoh K 2015 Material gain analysis of GeSn/SiGeSn quantum wells for mid-infrared Si-Based light sources based on many-body theory *IEEE J. Quantum Electron.* **51** 1–8